E-Article

Optimization of Biomass Composition Explains Microbial Growth-Stoichiometry Relationships

Oskar Franklin,[1,*] Edward K. Hall,[2] Christina Kaiser,[3] Tom J. Battin,[2] and Andreas Richter[3]

1. International Institute for Applied Systems Analysis (IIASA), A-2361 Laxenburg, Austria; 2. Department of Limnology, University of Vienna, Althanstrasse 14, A-1090, Vienna, Austria; 3. Department of Chemical Ecology, University of Vienna, Althanstrasse 14, A-1090, Vienna, Austria

Submitted June 1, 2010; Accepted September 17, 2010; Electronically published January 12, 2011

abstract: Integrating microbial physiology and biomass stoichiometry opens far-reaching possibilities for linking microbial dynamics to ecosystem processes. For example, the growth-rate hypothesis (GRH) predicts positive correlations among growth rate, RNA content, and biomass phosphorus (P) content. Such relationships have been used to infer patterns of microbial activity, resource availability, and nutrient recycling in ecosystems. However, for microorganisms it is unclear under which resource conditions the GRH applies. We developed a model to test whether the response of microbial biomass stoichiometry to variable resource stoichiometry can be explained by a trade-off among cellular components that maximizes growth. The results show mechanistically why the GRH is valid under P limitation but not under N limitation. We also show why variability of growth rate–biomass stoichiometry relationships is lower under P limitation than under N or C limitation. These theoretical results are supported by experimental data on macromolecular composition (RNA, DNA, and protein) and biomass stoichiometry from two different bacteria. In addition, compared to a model with strictly homeostatic biomass, the optimization mechanism we suggest results in increased microbial N and P mineralization during organic-matter decomposition. Therefore, this mechanism may also have important implications for our understanding of nutrient cycling in ecosystems.

Keywords: optimization model, mineralization, growth-rate hypothesis, RNA, biomass stoichiometry, microbial physiology.

Introduction

Ecological stoichiometry provides a powerful tool for integrating microbial physiology and stoichiometry with ecosystem processes. For example, the growth-rate hypothesis (GRH) predicts that growth rate increases with phosphorous concentration through changes in RNA content (Sterner 1995), which has been observed in organisms from microbes (Makino et al. 2003) to humans (Elser et al. 2007). Recent theoretical advances show that the GRH, coupled with the metabolic theory of ecology, can explain stoichiometric patterns across organism types (Allen and Gillooly 2009). The GRH also underlies the experimental methods used to estimate microbial activity on the basis of ribosomal RNA (rRNA) content (Leser et al. 1995). However, these methods and theories should be interpreted with care because observations (Flärdh et al. 1992; Binder and Liu 1998; Elser et al. 2003) show that the GRH is not universally valid, especially in microorganisms. The relationship between bacterial biomass stoichiometry and growth rate can vary within the same species (Chrzanowski and Kyle 1996; Makino et al. 2003; Chrzanowski and Grover 2008) and depend on which nutrient is limiting growth (Sepers 1986). The mechanisms behind this variability are not yet well understood. Moreover, it has been proposed that a general lack of theory limits progress in the field of microbial ecology (Prosser et al. 2007). Thus, developing theory and models is an important step in elucidating the mechanisms behind the variable stoichiometry of microorganisms and its implications for nutrient cycling in ecosystems.

The response of microbial growth to variation in resource stoichiometry has commonly been modeled with cellular quotas, that is, the Droop model (Droop 1968; Thingstad 1987). A phytoplankton model by Klausmeier et al. (2004), also based on quotas, took this approach one step further by adding mechanistic detail linking the minimum quotas to structural composition in terms of resource acquisition and growth machinery. More importantly, this model employed an optimization strategy of trade-offs between resource acquisition machinery and growth machinery to control biomass composition. Optimality assumptions are attractive because they provide an ecological (and/or evolutionary) rationale for model behavior. Whereas optimal-biomass-allocation principles have been widely used to explain the response of plants and animals to resource availability (e.g., Kozłowski et al.

* Corresponding author; e-mail: franklin@iiasa.ac.at.

Am. Nat. 2011. Vol. 177, pp. E29–E42.
0003-0147/2011/17702-52207$15.00.
DOI: 10.1086/657684

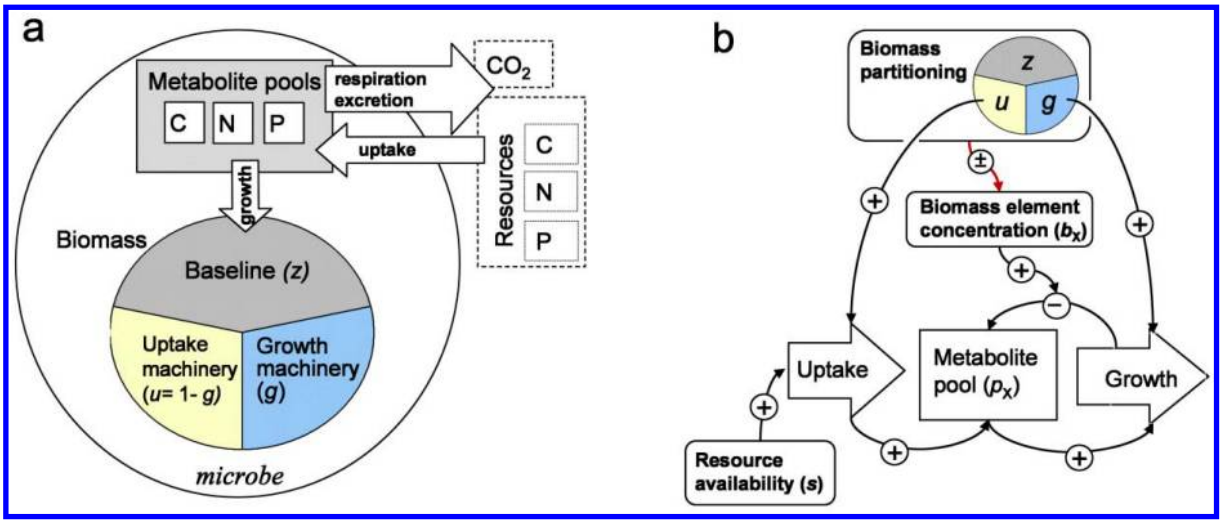

Figure 1: Model structure. *a*, Model components and fluxes (processes). *b*, Effect of biomass partitioning on cell processes for a growth-limiting element. Arrows indicate positive (*plus sign*), negative (*minus sign*), or variable (*plus-minus*) effect. Biomass composition (*u*, *g*, and *z*) has direct functional effects on growth and uptake and an indirect effect, through biomass element concentration, that affects nutrient metabolite consumption per unit of biomass growth (nutrient-use efficiency). For clarity, excretion (which is negligible for a limiting element) and respiration (which is constant) are not shown.

2004; Franklin et al. 2009), the few such studies that have been conducted for microorganisms are (to our knowledge) restricted to phytoplankton (e.g., Wirtz 2002; Klausmeier et al. 2004). For bacteria, proteome studies suggest trade-offs between growth and nutrient acquisition (e.g., Raman et al. 2005). However, the hypothesis that optimal allocation of cellular machinery explains the response of growth rate and biomass stoichiometry to resource stoichiometry in heterotrophic microorganisms has yet to be tested.

Here we take the optimization approach (Klausmeier et al. 2004) one step further in terms of mechanistic detail by explicitly modeling the growth process as a function of internal resource pools and cellular growth and uptake machinery, each with a fixed elemental composition. We hypothesize an optimal partitioning of biomass among growth machinery, uptake machinery, and other structural biomass. We then evaluate how optimization among these components affects biomass composition and stoichiometry under variable resource stoichiometry. Specifically, we show (1) that optimization of biomass composition that maximizes specific growth rate explains variability in bacterial biomass stoichiometry, (2) that resource stoichiometry strongly influences macromolecular composition (e.g., RNA content) so that the GRH is valid under P limitation but not under N limitation, and (3) that the presence of an optimization mechanism increases P and N recycling under C-limited bacterial growth, compared to that when biomass is strictly homeostatic.

Theory and Model

Model Structure and the Optimal-Biomass-Composition Hypotheses

In our model, structural biomass (fig. 1; table 1) is divided into cellular compartments with specific functions: (1) baseline biomass, denoted *z* (DNA, cellular membrane, cell wall, essential proteins), (2) growth machinery *g* (ribosomes, RNA), and (3) uptake machinery *u* (transmembrane proteins). In addition to structural biomass, we consider internal C, N, and P metabolite pools that are used for growth and respiration. All processes and variables (described below; table 2) are defined on a per-biomass basis, which allows us to not explicitly consider effects of cell volume or density changes. Unless indicated, biomass refers to the structural biomass only (excluding the internal metabolite pools).

For a given resource level (*s*), the relative partitioning of biomass among the three cell compartments (uptake machinery *u*, growth machinery *g*, and baseline biomass *z*) is adjusted to maximize the specific growth rate *G*. Specifically, the optimal cell composition depends on the balance between growth and uptake capacity and is further influenced by the elemental (C, N, P) demand for the construction of the selected biomass composition (fig. 1*b*). The fraction of baseline biomass *z* is, however, assumed to always be greater than a minimum value $z_{\min}$ to maintain essential functions other than growth and uptake. Adjustments of biomass composition, for example, amount

Table 1: Composition of cell compartments

Cell compartment	Symbol	Composition	Protein	C	N	P
Baseline biomass	z	Cell wall, membranes, DNA (15, 17[a])	62, ND[a]	43	14.9, 13.7[a]	1.0, 1.0[a]
Uptake machinery	u[b]	Protein	100	46	17	0
Growth machinery	g[b]	Ribosomal protein (33), RNA (67)[c]	33	37	15.3	5.87
C in metabolites	p_C	Carbohydrates (50), lipids (50)	0	54.2[d]	0	0
N in metabolites	p_N	NH_4 (50), amino acids (50)	0	23	47.4	0
P in metabolites	p_P	$NaPO_4$ (50), $NaPO_3$ (50)	0	0	0	28

Note: All values are in percent mass. Unless indicated, C, N, and P percentages in macromolecules and cell compartments are taken from Sterner and Elser (2002).

[a] Estimated from data for *Pectobacterium carotovorum* and *Escherichia coli*, respectively. ND = not determined.

[b] Mathematically, u and g are the uptake and growth fractions, respectively, of the nonbaseline biomass ($1 - z$).

[c] Assuming that 85% of RNA is in ribosomes and that ribosome RNA / protein = 1.8 for prokaryotes (Sterner and Elser 2002).

[d] From Vrede et al. (2004).

of RNA, have been shown to occur rapidly in response to environmental changes and in experiments (Kerkhof and Kemp 1999; Ferenci 2007). Thus, we assume that biomass composition is in dynamic equilibrium with the environmental conditions, although we also evaluate under which resource conditions the biomass composition may deviate from the optimal equilibrium-based predictions.

Cellular Compartments and Stoichiometry

The elemental composition of each cellular compartment (table 1) is based on values derived from the literature and original research presented in this study (see below). Only the elements C, N, and P are explicitly modeled, whereas all other atoms in biomass and metabolites are implicit. Specifically, the proportion of element X in biomass (b_X, where X denotes C, N, or P) is the product of the relative amount of each cellular compartment and its elemental content (X_g, X_u, X_z):

$$\begin{aligned} b_X &= z(X_z) + (1 - z)(gX_g + uX_u) \\ &= z(X_z) + (1 - z)[gX_g + (1 - g)X_u]. \end{aligned} \tag{1}$$

In equation (1), g and u are defined as fractions of the nonbaseline biomass, so that $u = 1 - g$. Resources are taken up from the environment and stored in metabolite pools that are represented by their C, N, and P contents, although the actual chemical forms of the resource pools (metabolites), for example, carbohydrates (C), amino acids (N, C), and phosphates (P), are variable. Nutrients are tapped from the metabolite pools (p) for growth of new biomass (G) and respiration (R) or are excreted (e.g., overflow metabolism E). Metabolite pools are assumed to be in dynamic equilibrium, so that their size depends on the balance between nutrient uptake (U) and use:

$$\begin{aligned} \frac{dp_X}{dt} &= U_X - Gb_X - E_X = 0, \\ \frac{dp_C}{dt} &= U_C - Gb_C - E_C - R = 0, \end{aligned} \tag{2}$$

where X represents N or P.

Cell Processes

Growth. The growth model is based on the synthesizing-unit (SU) concept, which is based on the microscopic interactions of growth machinery and different nutrients (app. A; Kooijman 1998, 2001). In our framework, the SU concept leads to a growth equation (eq. [3]) in which G increases with the ratio of metabolite concentration (p_X) to the demand of the same nutrient for biomass growth (controlled by b_X) until G approaches its maximum G_{max}:

$$\begin{aligned} \frac{db}{dt}\frac{1}{b} &= G \\ &= G_{max}\Bigg/\Bigg\{1 + \frac{G_{max}}{e_g}\Bigg[\frac{b_C}{p_C} + \frac{b_N}{p_N} + \frac{b_P}{p_P} - \left(\frac{p_C}{b_C} + \frac{p_N}{b_N}\right)^{-1} \\ &\qquad - \left(\frac{p_C}{b_C} + \frac{p_P}{b_P}\right)^{-1} - \left(\frac{p_P}{b_P} + \frac{p_N}{b_N}\right)^{-1} \\ &\qquad + \left(\frac{p_C}{b_C} + \frac{p_N}{b_N} + \frac{p_P}{b_P}\right)^{-1}\Bigg]\Bigg\}. \end{aligned} \tag{3}$$

In equation (3), e_g is the initial efficiency of the SU, that is, the growth per metabolite availability at low metabolite concentration (p_X), and G_{max} (maximum G) is proportional to the amount of growth machinery $g(1 - z)$ and its maximum capacity of biomass synthesis (f_G), which is a function of the maximal translational activity of the ribosomes (Jackson et al. 2008):

$$G_{max} = f_G(1 - z)g. \tag{4}$$

Table 2: Variables and parameters

Symbol	Unit[a]	Values[b]	Description
Variables:			
b_X	g X g B^{-1}	...	Fraction of element X in biomass
E_X	g X g B^{-1} h^{-1}	...	Specific rate of excretion of element X
g	...	...	Fraction of nonbaseline biomass in growth machinery
G	h^{-1}	...	Specific growth rate
p_X	g X g B^{-1}	...	Metabolite pool of element X
U_X	g X g B^{-1} h^{-1}	...	Resource uptake of element X
u	...	...	Fraction of nonbaseline biomass in uptake machinery
s_X	g X g B^{-1} h^{-1}	...	External resource level of element X
z	...	...	Fraction of baseline biomass of total structural biomass
Parameters:			
e_g	...	*P.c.*: .38; *E.c.*: 56	Maximum efficiency of the growth machinery
f_E	...	.01	Excretion rate factor
f_G	h^{-1}	*P.c.*: .93; *E.c.*: 4.2	Maximal synthetic capacity of the growth machinery
$p_{\lim X}$	g X g B^{-1}	*P.c.*: .43, .10, .021; *E.c.*: .42, .029, .0085	Theoretical maximum metabolite pools of C, N, and P, respectively
r	g C g B^{-1}	.02[c]	Baseline maintenance respiration
y	...	.5[d]	Growth efficiency: C growth per C used in the growth process
z_{min}	...	*P.c.*: .56; *E.c.*: .19	Minimum fraction of baseline biomass of total structural biomass

[a] B = structural biomass (biomass excluding the nutrient metabolite pools). X = any of the elements C, N, or P.

[b] *P.c.* and *E.c.* = *Pectobacterium carotovorum* and *Escherichia coli*, respectively. All parameter values are estimated from our data except as noted below.

[c] From Tännler et al. (2008).

[d] From Cajal-Medrano and Maske (1999).

It is commonly assumed that a single nutrient limits growth (cf. Liebig's law). In our model, this means that for the limiting nutrient, the ratio of the metabolite pool (p_X) to biomass concentration (b_X) is much smaller than that for the nonlimiting nutrients. Under these circumstances, equation (3) can be approximated by equation (5), which more clearly illustrates the interaction of G_{max} and each metabolite pool, that is, why small metabolite pools limit growth whereas G_{max} limits growth when metabolite pools are large:

$$G = \frac{G_{max}}{1 + (G_{max}/e_g)(b_X/p_X)}. \quad (5)$$

In equation [5], the subscript X refers to the most-limiting nutrient.

Uptake. Similar to the growth dynamics limited by G_{max}, resource uptake (U; eq. [6]) is limited by uptake capacity (U_{max}) at a high external resource level (s), whereas it is limited by s at low s (cf. Brandt et al. 2004; i.e., a Jacob Monod– or Michaelis-Menten-type functional form):

$$U_X = \frac{U_{max\,X} s_X}{U_{max\,X} + s_X}. \quad (6)$$

Here U_{max} is a function of uptake machinery (u), as defined below. Because we consider external resources solely in terms of their total effects on potential rate of element uptake, we can neglect underlying details of the uptake response to s, such as effects of different resource types. Instead, s represents the total effect of resource level on uptake, that is, s_X is the uptake of element X when the limitation by U_{max} is removed and U is completely resource limited. Uptake of a nonlimiting element is approximated by $U = U_{max}$ in our simulations.

Excretion and Respiration. To avoid having any element reach an unrealistic or deleterious concentration, there is an upper limit to the size of each internal nutrient pool (p; Russell and Cook 1995). If p approaches its upper limit (p_{lim}), then nutrients are excreted or rejected (for P and N) or respired (for C, overflow respiration) according to

$$E_X = \frac{f_E p_X}{p_{\lim X} - p_X} \quad (7)$$

(fig. B1). In equation (7), f_E controls how quickly E increases with p, and it is assumed to be low ($f_E = 0.01$) so that E is minimal below $p \to p_{lim}$.

Anabolic respiration associated with the construction of biomass (R_G) is proportional to growth (G); that is, $R_G = [1/(y - 1)]G$, where y is the growth efficiency (y = biomass C growth / total C used in the growth process). Although y may be variable among species and for different environmental conditions, differences in y have only

quantitative effects under C limitation but no qualitative effects on our results. Thus, for simplicity, we assume a growth efficiency of $y = 0.5$ (Cajal-Medrano and Maske 1999). Specific maintenance respiration (R_m) is assumed to be constant for each species (Pirt 1982) but varies among species. A linear relationship between maximum G and specific maintenance rate (R_m) has been observed across species (van Bodegom 2007); this can be explained by the energetic costs of protein synthesis machinery (here g) increasing with its translation speed (here f_G; Dethlefsen and Schmidt 2007). In our model, this relationship corresponds to R_m proportional to f_G, where $r = 0.02$ (Tännler et al. 2008) is the baseline respiration:

$$R_m = rf_G. \tag{8}$$

Balancing Capacities for Nutrient Uptake and Use. Uptake capacity and growth capacity are linked to their respective proportions (g and u) of the nonbaseline biomass ($1 - z$) through a trade-off ($u = 1 - g$), so that both capacities cannot be maximized simultaneously. Furthermore, given the benefits of the ability to utilize and buffer variations in resource supply (e.g., Thomas and O'Shea 2005), maximum uptake capacity should be higher than maximum growth capacity. Specifically, we assume that a reference uptake capacity, given by $u = u_0 = 0.5$, suffices to match maximum growth capacity (U_{max} at $g = u = 0.5$ equals $G_{max}b_X$ at $g = 1$) for each nutrient, which leads to equation (9). However, as long as the maximum uptake capacity is not smaller than maximum growth capacity, our results are not sensitive to this assumption.

$$U_{max\,X} = \frac{f_G b_X}{u_0}\, u\,(1 - z),$$

$$U_{max\,C} = \left[\frac{f_G b_C (1 - z_{min})}{y} + rf_G\right]\frac{u\,(1 - z)}{(1 - z_{min})u_0}, \tag{9}$$

for $X =$ N or P. In equation (9), b_X (eq. [1]) is evaluated at $g = u_0 = 0.5$ and $z = z_{min}$.

Model Evaluation

Solving for Optimal Biomass Composition. To evaluate the model, G (eq. [3]) was maximized with respect to biomass composition (g and z) for each substrate level (s), under the constraint $z > z_{min}$. We numerically solved for s to obtain optimal g and z as a function of G. In each case, single-element limitation was modeled; that is, only one resource element at a time affected G, while the effects of the other resources were fixed by setting their uptake rate $U = U_{max}$ (see "Uptake"). In addition, we evaluated the robustness of the optimal biomass composition in terms of the probability for suboptimal values of g and z. For example, because of rapid fluctuations in resource level, cells may not always be in dynamic equilibrium with the environment and may therefore deviate from the modeled optimal composition, which would lead to variation around the optimal G-to-g and G-to-z relationships. The range of this variability should be larger the less sensitive G is to deviation of g and z from their respective optima. Thus, as a measure of potential variability in g and z, we calculated how far each parameter can be from the optima without reducing G by more than 5%.

Model Testing and Evaluation. To test the most central assumption in the model, optimal biomass partitioning, we compared model predictions and data for concentrations of macromolecules specific to two of the three biomass compartments. The data came from a chemostat experiment using *Escherichia coli* (Makino et al. 2003) and a batch culture experiment using *Pectobacterium carotovorum* (app. C; Keiblinger et al. 2010). RNA was used as an index of growth machinery (as 85% of cellular RNA is rRNA; table 1), and DNA was used as an index of baseline biomass. To minimize the effect of changes in nonstructural components, that is, metabolite pools, we analyzed RNA and DNA relative to protein content (for *P. carotovorum*), which is not affected by metabolite pools. When protein data were not available (for *E. coli*), they were replaced by total N content. The model was fitted (see method below) to measured RNA : protein, DNA : protein, and P metabolite pool : protein for *P. carotovorum* and to RNA : N and DNA : N for *E. coli*. For the testing of metabolite pool dynamics we chose P, because we can more easily separate metabolites and structural components—that is, amounts in RNA (fixed proportion of growth machinery) and in baseline biomass (constant under P limitation; table 1)—for P than for C and N, which occur in all cell compartments and in more than one metabolite pool. For *P. carotovorum*, the limiting nutrient was identified for each treatment on the basis of measured dynamics of metabolite pools and storage (polyphosphate and carbohydrates) in response to growth rate (app. C). For *E. coli*, we relied on limitations identified in the original study (Makino et al. 2003). Finally, we evaluated the consequences of our optimization hypothesis for nutrient recycling during decomposition by simulating the effect of declining C availability, which is ubiquitous during organic-matter decomposition.

Parameterization. Although the elemental composition of the macromolecules and the macromolecular composition of the cellular compartments are constrained (Sterner and Elser 2002), some components vary among species or are difficult to estimate accurately from literature data. Thus,

we estimated species-specific values for minimum baseline biomass (z_{min}) and its N, protein, and DNA contents from data for each species. For the process-related parameters, we estimated species-specific values for the maximum capacity (f_G) and efficiency (e_g) of the growth machinery and the maximum metabolite pool sizes ($p_{lim\ X}$). Best-fit parameters (maximum likelihood of yielding the measured data) were estimated via Markov chain Monte Carlo (e.g., Gelman et al. 2004), which has the advantage, compared to standard optimum-seeking methods, of minimizing the risk of selecting a local but not global optimum for the parameter values. For all calculations we used MathCad (ver. 13) software (code available in a zip file).

Results: Model Performance and Behavior

Modeled and Measured Relationships between Growth Rate and Macromolecular Biomass Composition

In order to evaluate the presence of the hypothesized optimization mechanism, we compared measurements with model predictions (optimal and potential suboptimal ranges of variability) of covariation of biomass composition and specific growth rate induced by variation in resource level and resource C : N : P stoichiometry. Specifically, we tested for RNA : protein, DNA : protein, and P metabolite pools : protein ratios under N and P limitation for *Pectobacterium carotovorum*. For *Escherichia coli*, protein data were not available, so we tested for RNA : N and DNA : N under C and P limitation.

For *P. carotovorum*, the modeled biomass composition versus growth rate G differed significantly between N-limited growth and P-limited growth (fig. 2). Under P limitation, modeled RNA : protein increased linearly with G, in accordance with the growth-rate hypothesis (GRH). However, under N limitation, the modeled RNA : protein relationship with G was nonlinear and clearly defied the GRH. Also, the modeled DNA : protein ratio differed between P and N limitation. Whereas this ratio did not vary with G under P limitation, it increased with declining G under N limitation, resulting from a relative increase in baseline biomass (z, which includes DNA) and a relative reduction of both growth and uptake machinery. These model predictions of optimal biomass composition were consistent with the observed trends in RNA : DNA : protein ratios versus G, capturing the differences in these relationships between P and N limitation (fig. 2). In addition, most of the observed variability of the response variables was within the modeled range of potential variability (fig. 2, *thin lines*), although under P limitation some observed variability in DNA : protein could not be readily explained by the model. For *E. coli*, the model predicted linearly increasing RNA : N versus G under P limitation and a similar relationship, with a smaller slope, under C limitation over the range of observed G. For optimal DNA : N, no effect of G or difference between C and P limitation was predicted by the model. However, for both DNA : N and RNA : N the model suggests a higher potential variability under C limitation than under P limitation. These modeled trends for optimal biomass composition were again consistent with observations (fig. 2).

The modeled P metabolite pool in *P. carotovorum* differed significantly between P-limited and non-P-limited conditions, resulting in a much lower pool under P limitation than under N limitation (fig. 3). In addition, under P limitation the P metabolite pool increased strongly with increasing G, whereas such a monotonic relationship was not present under N limitation. The model implies that this difference reflects a general difference between the metabolite pool dynamics of limiting and nonlimiting nutrients. For a limiting nutrient, the metabolite pool (p) increases with G because p is a dominant control of G (fig. 1*b*; eq. [5]). In contrast, nonlimiting nutrients can accumulate in metabolite pools without strong effects on G. Instead, nonlimiting metabolites are passively controlled by the flux balance of the cell; for example, they are reduced through increased use when G increases at constant uptake capacity. This difference between limiting and nonlimiting conditions was confirmed by the measured trends in P metabolites in *P. carotovorum* (fig. 3).

The differences in estimated model parameters (the model interpretation of the empirical data) between the two bacterial species imply that *E. coli* reaches a higher G than does *P. carotovorum* because of the higher capacity (f_G) and higher efficiency (e_g) of its growth machinery. The difference in G is further enhanced by *E. coli*'s lower minimum requirement for baseline biomass (z_{min}). The model also suggests that the species differed in their maximum metabolite pools for P and N, although we were not able to evaluate this using the available empirical data.

In summary, the model predicted trends in the relationships among biomass G, RNA, DNA, and protein and how those relationships differed under C, N, and P limitation, in agreement with observations. This result is consistent with an optimization of biomass composition to maximize specific growth rate in response to resource levels. In addition, the agreement between modeled and measured dynamics of the metabolite pools was consistent with the growth and uptake mechanisms proposed in the model.

Implications for a Microbial Process, Nutrient Recycling

During microbial decomposition of organic matter, resource C : N and C : P ratios gradually decline because of the loss of C through microbial respiration. We evaluated the effect of our optimization hypothesis on this process

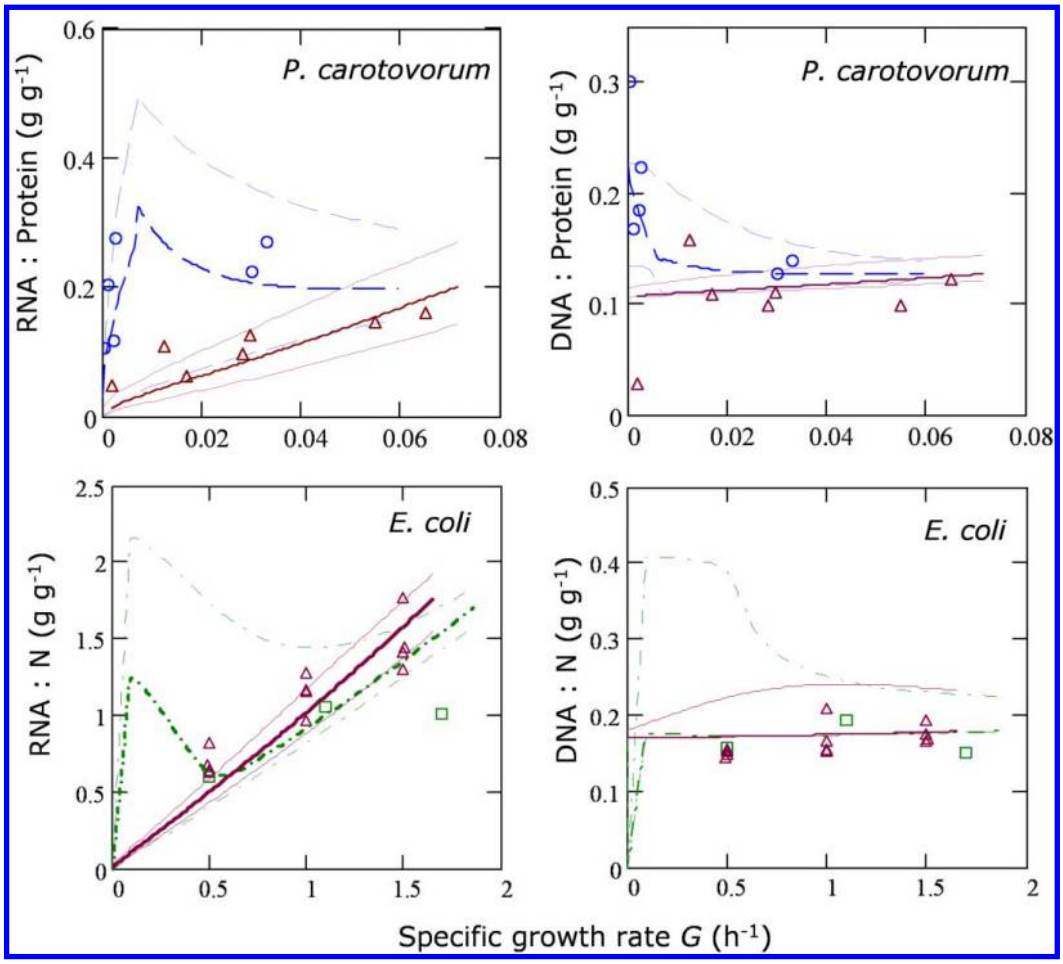

Figure 2: Relationships between biomass composition ratios and specific growth rate (G) induced by variation in external resource levels for two species of bacteria. Modeled (*lines*) and measured (*symbols*) results for growth under different single-element limitations: N limitation (*dashed lines*, *circles*), P limitation (*solid lines*, *triangles*), and C limitation (*dash-dotted lines*, *squares*). The optimal state (*thick middle line*) and intervals of near-optimal states (95% optimal; *upper and lower thin lines*) were modeled. The distance between the thin lines represents the range of near-optimal values. For *Pectobacterium carotovorum*, $r^2 = 0.79$ and 0.10 for RNA : protein and DNA : protein, respectively, under P limitation and 0.43 and 0.63, respectively, under N limitation. For *Escherichia coli*, $r^2 = 0.86$ and 0.31 for RNA : N and DNA : N, respectively, under P limitation, and 0.57 and 0.086, respectively, under C limitation.

for a bacterium (*P. carotovorum*) by model simulation of declining resource C level at two levels of fixed resource N availability and constant resource P (fig. 4).

Compared to the case when biomass was homeostatic, optimization of biomass composition led to a small increase in growth rate and a slight change in biomass C : N but a significant change in biomass N : P when C limitation set in. More importantly, modeled recycling (mineralization) of both N and P was increased because of the optimization. This is explained by the shift from a low proportion of uptake machinery (u) under N limitation to higher u under C limitation (mechanism explained below). This shift increases uptake and therefore also excretion of excess nonlimiting elements, that is, P and N. If the resource N level is reduced, the resource C : N ratio where the shift to C limitation occurs is increased. This effect of resource N level is due to the effect of maintenance respiration that causes a growth-independent C-use term, which means that total C use does not decline in proportion to N use as resource N level declines.

Discussion

Mechanisms Regulating the Contrasting Biomass Composition among P, N, and C Limitation

In both the model and the empirical studies, growth rate (G) scaled consistently with RNA and biomass P content

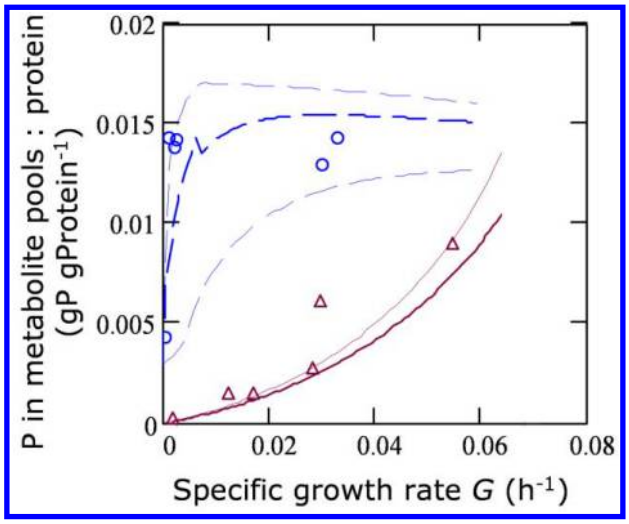

Figure 3: Relationships between metabolite pool phosphorus : biomass protein ratio and specific growth rate (G) induced by variation in external resource levels. The growth-limiting elements were nitrogen (N) and phosphorus (P; symbols and lines as in fig. 2). The lower thin solid line for P limitation (near-optimal value) coincides with the thick solid line (optimal value). Measured P metabolite pools were calculated from the P budget as $P_{total} - P_{RNA} - P_z$, where $P_z = P_{DNA} + P_{z\,non\text{-}DNA}$. $P_{z\,non\text{-}DNA}$ was the non-DNA P content in baseline biomass (z) and was estimated as 0.28% by fitting the y-intercept of the metabolite pool versus G under P limitation to 0. For P limitation, one outlier, at $G = 0.065$, for which the estimated P metabolite pool was <0 was removed from the analysis. $r^2 = 0.32$ and 0.87 under N and P limitation, respectively.

under P limitation and, at higher growth rates, under C limitation, but not under N limitation. To understand these differences, it is important to understand the two interacting mechanisms through which biomass partitioning maximizes growth rate in our model. First, changes in proportions of growth and uptake machinery (g and u, respectively) cause a functional trade-off between growth and uptake capacity. Second, the resultant changes in biomass composition affect the demand for (use of) the limiting element per biomass constructed; that is, a nutrient-use efficiency (NUE) effect emerges. This effect determines the rate at which the metabolite pool is depleted for a given growth rate (fig. 1*b*). While the functional trade-off always supports the GRH, the NUE effect does not. The NUE effect is important at low resource levels, where it results in biomass patterns that are consistent with the GRH under P limitation but not under N limitation. Therefore, resource level ultimately determines which mechanism controls the relationship between biomass stoichiometry and growth.

The optimization of the functional trade-off acts equally for all limiting elements, by favoring growth machinery at the expense of uptake machinery as resource level increases. At a high resource level, this optimization of functional capacity is the dominant mechanism controlling biomass composition. Under these conditions, the positive relationships between RNA, G, and biomass P may emerge independently of which element is limiting, consistent with the GRH. Baseline biomass z will always be at its minimum value because it does not contribute to either uptake or growth capacity.

At declining resource levels, the effects of uptake and growth capacity decline because uptake is controlled by resource level rather than uptake capacity (fig. 1*b*; eq. [6]). As a consequence, the relative importance of the NUE effect increases and biomass is allocated toward the compartment with the lowest concentration of the limiting nutrient. For example, under P limitation, because uptake machinery is lowest and growth machinery highest in P, the NUE effect reinforces the functional trade-off that reduces growth machinery as available P decreases. In contrast, under N limitation, the NUE effect opposes the functional effect because the growth machinery has an N concentration lower than that of the uptake machinery, leading to increasing allocation to the growth machinery (RNA) even though growth rate is declining. However, at very low resource levels, increased baseline biomass z will be favored because of its even lower N concentration, despite the fact that this reduces both uptake and growth capacity. Together, these responses provide a mechanistic explanation for couplings between growth and biomass stoichiometry that lead to the non-GRH-compliant relationships observed under N limitation (fig. 2).

Under C limitation, there is an NUE effect analogous to but smaller than that under N limitation (because growth machinery is lower in C than is uptake machinery). However, under C limitation, maintenance respiration becomes an important determinate of biomass C at a low growth rate, which limits the importance of the NUE effect and maintains GRH-compliant relationships except at very low growth rates (fig. 2).

Mechanisms Regulating Potential Suboptimal Variability in Biomass Composition

The modeled differences in the near-optimal ranges (the distance between the thin lines in fig. 2) under limitation by different nutrients suggests that the relationship between optimized g and the specific growth rate (and therefore the RNA-G relationship) is much less constrained and more prone to variation at low G under C limitation and under N limitation than under P limitation. For example, the near-optimal range of RNA : protein under N limitation is ~10 times that under P limitation at a low growth rate for *Pectobacterium carotovorum* (fig. 2). This difference

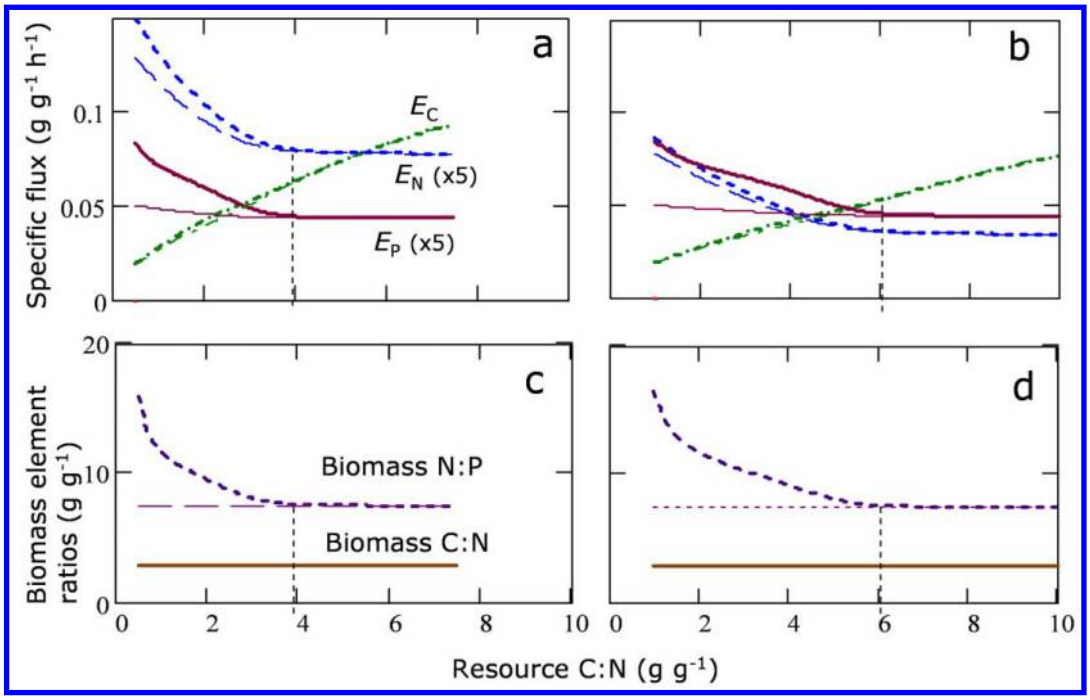

Figure 4: Simulated C, N, and P recycling (E_C, E_N, and E_P) and bacterial (*Pectobacterium carotovorum*) biomass element ratios in response to external resource C : N ratio. The difference between homeostatic structural biomass (*thin lines*) and dynamically optimized biomass partitioning (*thick lines*) was tested. Resource C : N was varied by reducing C availability from right to left on the *X*-axis, which caused a shift from N limitation to C limitation of bacterial growth (P was not limiting). The approximate shifting points are indicated by vertical dashed lines. *a*, *b*, Recycling (*E*) of C (*dash-dotted lines*), N (× 5; *dashed lines*), and P (× 5; *solid lines*). *c*, *d*, Structural biomass element ratios for C : N (*solid line*) and N : P (*dashed line*). *a* and *c* correspond to double the resource N level in *b* and *d*.

is due to the interaction of the NUE effect and the functional effect on the optimal biomass allocation. Under P limitation these mechanisms work together, amplifying the effect of P use on growth, whereas under N limitation they oppose each other and therefore tend to cancel out. This difference leads to a high sensitivity of *G* to P use and therefore to variation in biomass composition (*g* and *z*) under P limitation, while under N limitation the corresponding sensitivity of *G* to biomass composition is low.

Novel Aspects and Implications for Microbial Biomass Stoichiometry

Our model links physiology directly to biomass composition and therefore to biomass stoichiometry, employing optimization of structure composition as the controlling mechanism. We have shown that the optimization strategy, rooted in an ecological and evolutionary rationale, provides a means to understand how microbial biomass stoichiometry and physiology are influenced by changes in the environment, including resource variation. In addition to the novel optimization strategy, our model differs from widely used microbial stoichiometry models (e.g., quota models: Droop 1968; Thingstad 1987) in its more mechanistic representation of the growth process, which describes gradual shifts between different resource limitations and the explicit interaction of growth machinery and metabolite pools. Supported by empirical data, we showed how this interaction leads to a positive concave relationship between *G* and the metabolite pool for a limiting nutrient, while the metabolite pool tends to decrease with *G* at high *G* for nonlimiting nutrients (fig. 3). Our model provides a mechanistic explanation for such relationships, which also have been observed for different nutrients in yeast (Boer et al. 2010).

We applied the model to elucidate observed patterns of covariation among biomass composition, stoichiometry, and growth, such as the growth-rate hypothesis (GRH), under different resource stoichiometry. Integration of stoichiometric theory, cellular composition, and physiology has previously been done on the basis of the GRH (Vrede et al. 2004) and by incorporating the GRH into the metabolic theory of ecology (Allen and Gillooly 2009). However, while the resulting theory explained patterns across organism types, it did not explain how individual organisms and populations adapt or acclimate to changes in

resource level and stoichiometry. By contrast, adaptive phenotypic plasticity, that is, optimal acclimation of biomass composition, is central in our model. Moreover, multiple empirical studies show that a theory where ribosome content always correlates with growth seems insufficient for dealing with microorganisms, because they often defy the GRH under non-P limitation (Flärdh et al. 1992; Binder and Liu 1998; Elser et al. 2003). In the light of our model, such results are explained by opposing effects of biomass composition on functional capacities versus nutrient-use efficiency, exemplified for *P. carotovorum* under N limitation (fig. 2). In addition, at low G under C and particularly N limitation, our model implies that G is relatively insensitive to variation in cell composition (fig. 2), suggesting an explanation for the high variability in stoichiometric relationships and RNA observed under these conditions. Thus, our model offers a mechanistic explanation for observations of variable and high RNA abundance at low G, which has previously been suggested to be a means of responding quickly to increased resource levels (Flärdh et al. 1992). Our suggested mechanism may also have contributed to the decoupling of growth-rate RNA and biomass P observed in bacteria across a large number of lakes (Hall et al. 2009).

Although our results are consistent with the limited validity of the GRH observed under many resource conditions, they do not imply that the GRH is exclusively restricted to P limitation, as suggested by Elser et al. (2003). We showed that organisms grown under C limitation (*Escherichia coli*; fig. 2) can give rise to a relationship between G and RNA similar to that under P limitation. However, in contrast to P limitation, under C limitation such relationships result from a purely functional trade-off between uptake and growth capacity and are not affected by nutrient- (here C-) use efficiency (NUE). Although not shown, the functional trade-off also leads to GRH-compliant relationships under "balanced growth," that is, when all nutrients are colimiting, because there is no opposing effect of NUE, as there is no benefit of increasing the NUE of any particular nutrient relative to other nutrients. In agreement with these predictions, the GRH has been verified for a range of microorganisms under balanced growth or C limitation (Karpinets et al. 2006).

The relationship between RNA and G varied significantly between *E. coli* and *P. carotovorum* (fig. 2), supporting empirical results that show that this relationship is stronger within a species than across species (Kemp et al. 1993; Kerkhof and Kemp 1999) or communities (Hall et al. 2009). Furthermore, our model implies that this relationship is strongly linked to the capacity of the growth machinery, that is, the maximal synthetic capacity of RNA (f_G; eqq. [3]–[5]), which differs strongly between our investigated species (table 2). This result explains mechanistically why the synthetic capacity of rRNA is a key factor controlling differences in the RNA-G relationship across species with different ecological strategies, as has been proposed (Dethlefsen and Schmidt 2007). These interspecies differences may also be reinforced by differences in the proportion of biomass not related to growth or uptake (z), which we predicted to be much higher for the slower-growing *P. carotovorum* than for the fast-growing *E. coli*.

Implications for Nutrient Cycling

Nutrient recycling (mineralization) is in large part a microbial process that is strongly affected by the stoichiometry of microbial biomass (Cherif and Loreau 2007; Manzoni et al. 2008). Because our growth mechanism (eq. [3]) is based on the synthesizing-unit concept (Kooijman 1998, 2001), it readily models the gradual shift from N to C limitation of microbial growth that gradually enhances the N (and P) mineralization : immobilization ratio during the decomposition process. Our results indicate that the excretion of N and P during organic-matter decomposition is increased if biomass is dynamically optimized relative to excretion when biomass is strictly homeostatic. Therefore, our model results suggest that part of nutrient mineralization during organic-matter decomposition is a by-product of microorganisms adjusting their biomass composition to maximize growth (fig. 4). Thus, our suggested optimization mechanism may allow us to develop a better understanding of nutrient mineralization and immobilization dynamics in ecosystems.

Limitations and Possibilities for Additional Evaluation

Our ability to validate all aspects of the model for a wider range of microorganisms was limited by the availability of data that included all necessary biomass compartments, growth rate, and a conclusive identification of the limiting nutrient. In particular, direct evidence for changes in uptake capacity would be valuable for additional testing of the model and the potential effects on nutrient recycling. However, while the link between growth machinery and RNA is well established, a measure of uptake machinery is not readily obtainable from macromolecular composition. The application of stable-isotope probing and single-cell techniques to microbial ecology may allow for higher resolution and more specific estimates of uptake dynamics in future studies (Wagner 2009).

Although our data support our assumption that the metabolite pools are in equilibrium with the growth rate (fig. 3), this may not always be the case, for example, under rapid variations in resource level. However, if the equilibrium assumption (eq. [2]) is relaxed, the model should

also be valid under nonequilibrium conditions, which would be an interesting topic for further analysis.

Conclusions

Our analysis suggests that maximization of specific growth rate G, constrained by a trade-off between growth and uptake capacity, is a dominant control on bacterial biomass composition. In addition, the shifts in biomass composition affect the resource demands for a given growth rate, that is, nutrient-use efficiency, because the elemental composition of each cellular component is unique. These two mechanisms can be complementary, as under P limitation, and can strengthen the relationship between growth and biomass stoichiometry. They can also act antagonistically, for example, under N limitation. At a low resource level, where nutrient-use efficiency becomes a more important control than the functional growth-uptake trade-off, the nutrient-use efficiency optimization will lead to different biomass allocation patterns, depending on which nutrient is limiting. For example, the growth-rate hypothesis (GRH) is valid under P limitation but breaks down under N limitation. The elucidation of these specific mechanisms provides the first clear mechanistic explanation for why GRH relationships can come uncoupled under certain resource stoichiometry conditions. In addition, the model results suggest that optimization of cellular composition during decomposition of organic matter indirectly increases N and P mineralization. Such dynamics may play an important role in nutrient cycling in ecosystems.

The ability of the model to mechanistically predict bacterial biomass stoichiometry and the model's potential implications for nutrient recycling suggest that its mechanisms may be an appropriate starting point for incorporating dynamic microbial physiology into ecosystem-level models. Because our model is rooted in an ecological and evolutionary rationale, it can be used to mechanistically explain patterns of microbial stoichiometry in an ecological context. In addition to established empirical patterns of what happens (e.g., biomass P : N ratio increases with G), the model explains when it happens (e.g., under C limitation), how it happens (e.g., a growth-uptake trade-off), and why it happens (ecological optimization).

Acknowledgments

This work is a contribution from the Austrian national research network MICDIF (Linking Microbial Diversity and Functions across Scales and Ecosystems) and was supported by the Austrian Science Foundation (Fonds zur Förderung der wissenschaftlichen Forschung, grant S10008-BI7) and IIASA, the International Institute of Applied Systems Analysis.

APPENDIX A

The Synthesizing Unit (SU) and Growth

An SU is analogous to an enzyme to which substrate molecules bind to form a product that is then released (Kooijman 1998, 2001). In our case, the product is biomass and the substrates are carbon (C), nitrogen (N), and phosphorus (P); all other atoms in biomass and substrate are implicit. The SU has binding sites for all substrate molecules, such that all sites must bind substrate before the product is released. The production rate of the SU depends on the probabilities per time unit that the substrate molecules bind (substrate flux) relative to the number of binding sites. In our model, the relative number of binding sites among elements in the SU mirrors the content of the elements in biomass (b_X). The substrate flux (binding probability) is proportional to the metabolite concentrations for each nutrient (p_X). This formulation is based on an SU model simplified for production of a generalized compound (biomass) limited by three substrates (C, N, and P; Kooijman 1998).

The above describes the growth properties per unit growth machinery (corresponding to 1 SU). To incorporate the effects of variable amounts of growth machinery (many SUs), we apply basic Michaelis-Menten-type kinetics. At low amounts of growth machinery relative to p, specific growth (G) is limited by $G_{\max}$ (eq. [4]), which is proportional to the amount of growth machinery $g(1 - z)$ and its maximum capacity for biomass synthesis (f_G), which is a function of the maximal translational activity of the ribosomes (see Jackson et al. 2008). At high amounts of growth machinery relative to metabolite concentration, many units of growth machinery compete for little substrate, so that G is not limited by the amount of growth machinery but by its efficiency (e_g), that is, the product formation of each SU per nutrient flux.

APPENDIX B

Modeled Growth and Excretion

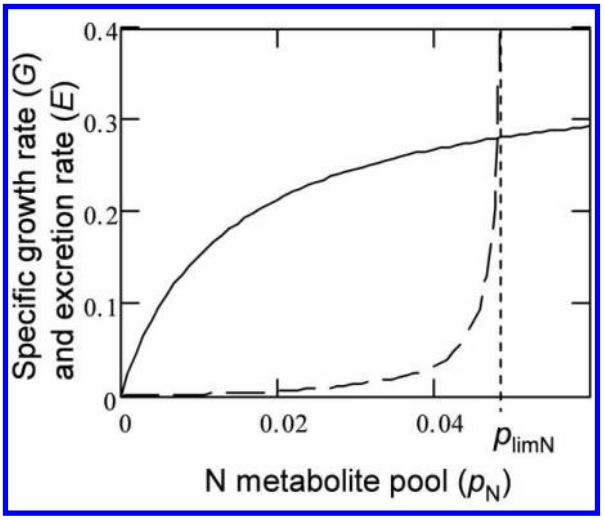

Figure B1: Modeled microbial growth (*solid line*) and excretion (*dashed line*) as functions of the internal nutrient metabolite pool (p_N). Excretion prevents p_N from exceeding the maximum $p_N = p_{limN}$ (*dotted vertical line*).

APPENDIX C

Experiment for *Pectobacterium carotovorum*

Treatments

Pectobacterium carotovorum (Bergey et al. 1923, pp. 374–375) was cultivated in batch cultures, in three replicates, in liquid minimal media modified from the one used by Clark and Maaløe (1967). The media contained 30 mM MOPS (pH 7.0), 0.1 nM $CaCl_2$ 0.1, 3 μM $FeSO_4$, 20 mM KCl, 2 mM $MgCl_2$, 14 mM Na_2SO_4, and 51 mM NaCl. Glucose, NH_4Cl, and Na_2HPO_4 were added as carbon (C), nitrogen (N), and phosphorus (P) sources, respectively, in different amounts and ratios, giving a total of 12 combinations (treatments) of C, N, and P. Bacterial media were sterilized by autoclaving at 121°C for 20 min. Glucose was added to autoclaved media from filter-sterilized (pore size: 0.2 μm) stock solutions. The inoculations on the media were made from precultures grown for 60 h in the respective minimum media with fixed concentrations of 150 mM C, 12.5 mM N, and 0.25 mM P. The precultures were then centrifuged; the pellets were washed twice with minimal media without C, N, or P sources and then resuspended once more in minimal media to inoculate the 12 treatments. Cultivation was performed in 400 mL of media at 22°C on a rotary shaker at 180 rpm. For determination of biomass and its elemental composition, each of the 12 treatments was run in 400 mL of either three or four replicates as described above. For each treatment, the bacterial cultures were measured at two growth phases, logarithmic (initial fast growth) and stationary (late slow, strongly resource-limited growth).

Measurements

The bacterial cultures were transferred into centrifuge flasks and centrifuged for 45 min at 10,845 *g*. The biomass pellet was washed twice with 50 mL of 130 mM NaCl, followed by resuspension in 50 mL of 130 mM NaCl and centrifugation for 10 min at 10,845 *g*. The biomass was dried in a drying oven for determination of dry mass and C, N, and P content. Aliquots of dried biomass (~2 mg) were weighed into tin capsules, and total C and N were determined with an elemental analyzer (EA 1110, CE Instruments, Milan, Italy). For analysis of total P in biomass, approximately 10 mg of dried samples were wet digested with 1 mL of nitric acid–perchloric acid mixture (4 : 1 ratio of HNO_3 to $HClO_3$; Kolmer et al. 1951, pp. 1090–1091) in 2-mL glass flasks on a heating plate. For acid digestion, the temperature was increased stepwise to 250°C and then maintained until a small residual volume was left in the glass flask. Samples were cooled to room temperature and filled to the 2-mL level with milliQ water. Inorganic P in the digests was quantified photometrically on the basis of the phosphomolybdate blue reaction (Schinner et al. 1993) in a microtiter plate format with a microplate reader (BIOTEK Instruments). RNA content was measured by fluorometry with the fluorescent stain RiboGreen according to the methods of Makino and Cotner (2004). The growth rates were determined by measuring the increase in turbidity. Turbidity was monitored at regular intervals with a microplate reader with 250-μL aliquots at a wavelength of 450 nm for bacteria. Optical density (OD) growth kinetics was constructed by plotting the OD of suspensions corrected for noninoculated medium versus time of incubation. At biomass densities higher than OD > 0.6, the samples were diluted.

Calculation of Growth Rate and Identification of Limiting Resource

The bacterial growth rate was determined by using a five-parameter logistic growth model that was fitted (using the Levenberg-Marquardt algorithm in the software SigmaPlot) to measured OD as a function of time. Specific growth rate (G) was evaluated for each biomass sampling point t_s as growth in OD divided by OD; that is, $G = [(d\mathrm{OD}/dt)/\mathrm{OD}]$ at $t = t_s$. Observations at extremely low

growth rates not significantly different from 0 were excluded because of the high uncertainty in the growth-rate estimate.

The change in non–nucleic acid P ($P_{total} - P_{RNA} - P_{DNA} \approx$ nonstructural, metabolite P) with growth rate between the two growth phases was used to detect the limiting resource. According to our theory, P limitation was indicated by decreased non–nucleic acid P concentration during the transition from initial (fast) to late (slow) growth. The results were also confirmed by an analysis of polyphosphate (indicative of P storage). Absence of P limitation was interpreted as N limitation. Carbon limitation was excluded because carbohydrate concentration (indicating C storage) increased between the logarithmic and stationary phases in all treatments.

Literature Cited

Allen, A. P., and J. F. Gillooly. 2009. Towards an integration of ecological stoichiometry and the metabolic theory of ecology to better understand nutrient cycling. Ecology Letters 12:369–384.

Bergey, D. H., F. C. Harrison, R. S. Breed, B. W. Hammer, and F. M. Huntoon. 1923. Bergey's manual of determinative bacteriology. Williams & Wilkins, Baltimore.

Binder, B. J., and Y. C. Liu. 1998. Growth rate regulation of rRNA content of a marine *Synechococcus* (cyanobacterium) strain. Applied and Environmental Microbiology 64:3346–3351.

Boer, V. M., C. A. Crutchfield, P. H. Bradley, D. Botstein, and J. D. Rabinowitz. 2010. Growth-limiting intracellular metabolites in yeast growing under diverse nutrient limitations. Molecular Biology of the Cell 21:198–211.

Brandt, B. W., F. D. L. Kelpin, I. M. M. van Leeuwen, and S. A. L. M. Kooijman. 2004. Modelling microbial adaptation to changing availability of substrates. Water Research 38:1003–1013.

Cajal-Medrano, R., and H. Maske. 1999. Growth efficiency, growth rate and the remineralization of organic substrate by bacterioplankton: revisiting the Pirt model. Aquatic Microbial Ecology 19:119–128.

Cherif, M., and M. Loreau. 2007. Stoichiometric constraints on resource use, competitive interactions, and elemental cycling in microbial decomposers. American Naturalist 169:709–724.

Chrzanowski, T. H., and J. P. Grover. 2008. Element content of *Pseudomonas fluorescens* varies with growth rate and temperature: a replicated chemostat study addressing ecological stoichiometry. Limnology and Oceanography 53:1242–1251.

Chrzanowski, T. H., and M. Kyle. 1996. Ratios of carbon, nitrogen and phosphorus in *Pseudomonas fluorescens* as a model for bacterial element ratios and nutrient regeneration. Aquatic Microbial Ecology 10:115–122.

Clark, D. J., and O. Maaløe. 1967. DNA replication and division cycle in *Escherichia coli*. Journal of Molecular Biology 23:99–112.

Dethlefsen, L., and T. M. Schmidt. 2007. Performance of the translational apparatus varies with the ecological strategies of bacteria. Journal of Bacteriology 189:3237–3245.

Droop, M. R. 1968. Vitamin B_{12} and marine ecology. IV. The kinetics of uptake, growth and inhibition in *Monochrysis lutheri*. Journal of the Marine Biology Association of the United Kingdom 48:689–733.

Elser, J. J., K. Acharya, M. Kyle, J. Cotner, W. Makino, T. Markow, T. Watts, et al. 2003. Growth rate–stoichiometry couplings in diverse biota. Ecology Letters 6:936–943.

Elser, J. J., M. M. Kyle, M. S. Smith, and J. D. Nagy. 2007. Biological stoichiometry in human cancer. PLoS ONE 2:e1028.

Ferenci, T. 2007. Bacterial physiology, regulation and mutational adaptation in a chemostat environment. Advances in Microbial Physiology 53:169–229, 315.

Flärdh, K., P. S. Cohen, and S. Kjelleberg. 1992. Ribosomes exist in large excess over the apparent demand for protein synthesis during carbon starvation in marine *Vibrio* sp. strain CCUG 15956. Journal of Bacteriology 174:6780–6788.

Franklin, O., R. E. McMurtrie, C. M. Iversen, K. Y. Crous, A. C. Finzi, D. T. Tissue, D. S. Ellsworth, R. Oren, and R. J. Norby. 2009. Forest fine-root production and nitrogen use under elevated CO_2: contrasting responses in evergreen and deciduous trees explained by a common principle. Global Change Biology 15:132–144.

Gelman, A., J. B. Carlin, H. S. Stern, and D. B. Rubin. 2004. Bayesian data analysis. Chapman & Hall/CRC, Boca Raton, FL.

Hall, E. K., A. R. Dzialowski, S. M. Stoxen, and J. B. Cotner. 2009. The effect of temperature on the coupling between phosphorus and growth in lacustrine bacterioplankton communities. Limnology and Oceanography 54:880–889.

Jackson, J. H., T. M. Schmidt, and P. A. Herring. 2008. A systems approach to model natural variation in reactive properties of bacterial ribosomes. BMC Systems Biology 2:62.

Karpinets, T. V., D. J. Greenwood, C. E. Sams, and J. T. Ammons. 2006. RNA : protein ratio of the unicellular organism as a characteristic of phosphorous and nitrogen stoichiometry and of the cellular requirement of ribosomes for protein synthesis. BMC Biology 4:30.

Keiblinger, K. M., E. K. Hall, W. Wanek, U. Szukics, I. Hämmerle, G. Ellersdorfer, S. Böck, et al. 2010. The effect of resource quantity and resource stoichiometry on microbial carbon use efficiency. FEMS Microbiology Ecology 73:430–440.

Kemp, P. F., S. Lee, and J. LaRoche. 1993. Estimating the growth rate of slowly growing marine bacteria from RNA content. Applied and Environmental Microbiology 59:2594–2601.

Kerkhof, L., and P. Kemp. 1999. Small ribosomal RNA content in marine proteobacteria during non-steady-state growth. FEMS Microbiology Ecology 30:253–260.

Klausmeier, C. A., E. Litchman, T. Daufresne, and S. A. Levin. 2004. Optimal nitrogen-to-phosphorus stoichiometry of phytoplankton. Nature 429:171–174.

Kolmer, J. A., E. H. Spaulding, and H. W. Robinson. 1951. Approved laboratory techniques. Appleton Century Crafts, New York.

Kooijman, S. A. L. M. 1998. The synthesizing unit as model for the stoichiometric fusion and branching of metabolic fluxes. Biophysical Chemistry 73:179–188.

———. 2001. Quantitative aspects of metabolic organization: a discussion of concepts. Philosophical Transactions of the Royal Society B: Biological Sciences 356:331–349.

Kozłowski, J., M. Czarnołęski, and M. Dańko. 2004. Can optimal resource allocation models explain why ectotherms grow larger in cold? Integrative and Comparative Biology 44:480–493.

Leser, T. D., M. Boye, and N. B. Hendriksen. 1995. Survival and activity of *Pseudomonas* sp. strain B13(FR1) in a marine microcosm determined by quantitative PCR and an rRNA-targeting probe and its effect on the indigenous bacterioplankton. Applied and Environmental Microbiology 61:1201–1207.

Makino, W., and J. B. Cotner. 2004. Elemental stoichiometry of a

heterotrophic bacterial community in a freshwater lake: implications for growth- and resource-dependent variations. Aquatic Microbial Ecology 34:33–41.

Makino, W., J. B. Cotner, R. W. Sterner, and J. J. Elser. 2003. Are bacteria more like plants or animals? growth rate and resource dependence of bacterial C : N : P stoichiometry. Functional Ecology 17:121–130.

Manzoni, S., R. B. Jackson, J. A. Trofymow, and A. Porporato. 2008. The global stoichiometry of litter nitrogen mineralization. Science 321:684–686.

Pirt, S. J. 1982. Maintenance energy: a general model for energy-limited and energy sufficient growth. Archives of Microbiology 133:300–302.

Prosser, J. I., B. J. M. Bohannan, T. P. Curtis, R. J. Ellis, M. K. Firestone, R. P. Freckleton, J. L. Green, et al. 2007. The role of ecological theory in microbial ecology. Nature Reviews Microbiology 5:384–392.

Raman, B., M. P. Nandakumar, V. Muthuvijayan, and M. R. Marten. 2005. Proteome analysis to assess physiological changes in *Escherichia coli* grown under glucose-limited fed-batch conditions. Biotechnology and Bioengineering 92:384–392.

Russell, J. B., and G. M. Cook. 1995. Energetics of bacterial growth: balance of anabolic and catabolic reactions. Microbiological Reviews 59:48–62.

Schinner, F., R. Öhlinger, E. Kandeler, and R. Margesin. 1993. Bodenbiologische Arbeitsmethoden. 2nd ed. Springer, Berlin.

Sepers, A. B. J. 1986. Effect of variable nutrient supply rates on the RNA level of a heterotrophic bacterial strain. Current Microbiology 13:333–336.

Sterner, R. W. 1995. Elemental stoichiometry of species in ecosystems. Pages 240–252 *in* C. Jones, and J. Lawton, eds. Linking species and ecosystems. Chapman & Hall, New York.

Sterner, R. W., and J. J. Elser. 2002. Ecological stoichiometry: the biology of elements from molecules to the biosphere. Princeton University Press, Princeton, NJ.

Tännler, S., S. Decasper, and U. Sauer. 2008. Maintenance metabolism and carbon fluxes in *Bacillus* species. Microbial Cell Factories 7: 19.

Thingstad, F. 1987. Utilization of N, P, and organic C by heterotrophic bacteria. I. Outline of a chemostat theory with a consistent concept of "maintenance" metabolism. Marine Ecology Progress Series 35: 99–109.

Thomas, M. R., and E. K. O'Shea. 2005. An intracellular phosphate buffer filters transient fluctuations in extracellular phosphate levels. Proceedings of the National Academy of Sciences of the USA 102: 9565–9570.

van Bodegom, P. 2007. Microbial maintenance: a critical review on its quantification. Microbial Ecology 53:513–523.

Vrede, T., D. R. Dobberfuhl, S. A. L. M. Kooijman, and J. J. Elser. 2004. Fundamental connections among organism C : N : P stoichiometry, macromolecular composition, and growth. Ecology 85: 1217–1229.

Wagner, M. 2009. Single-cell ecophysiology of microbes as revealed by Raman microspectroscopy or secondary ion mass spectrometry imaging. Annual Review of Microbiology 63:411–429.

Wirtz, K. W. 2002. A generic model for changes in microbial kinetic coefficients. Journal of Biotechnology 97:147–162.

Associate Editor: Volker Grimm
Editor: Mark A. McPeek

Transmission electron microscopy image of bacteria (*Pectobacterium carotovorum*) used in the study. The dark blue centers of the cells contain the cellular machinery and pools of storage compounds, which both adapt to the external resource availability. Photograph by Edward K. Hall.